AFCRL-65-222

ANTENNA LABORATORY REPORT NO. 65-3

ENERGY CONSIDERATIONS IN OPEN AND CLOSED WAVEGUIDES

by
S. LAXPATI
R. MITTRA

June 1965

Contract No. AF19(628)-3819
Project No. 4600
Task No. 460004
Technical Report No. 4.

Prepared For
AIR FORCE CAMBRIDGE RESEARCH LABORATORIES
OFFICE OF AEROSPACE RESEARCH
UNITED STATES AIR FORCE
BEDFORD, MASSACHUSETTS

ANTENNA LABORATORY
DEPARTMENT OF ELECTRICAL ENGINEERING
ENGINEERING EXPERIMENT STATION
UNIVERSITY OF ILLINOIS
URBANA, ILLINOIS

AFCRL-65-222 Antenna Laboratory Report No. 65-3

ENERGY CONSIDERATIONS IN OPEN AND CLOSED WAVEGUIDES

by

S. Laxpati
R. Mittra

June 1965

Contract No. AF19(628)-3819
Project 4600
Task 460004
Technical Report No. 6

Prepared for

AIR FORCE CAMBRIDGE RESEARCH LABORATORIES
OFFICE OF AEROSPACE RESEARCH
UNITED STATES AIR FORCE
BEDFORD, MASSACHUSETTS

DEPARTMENT OF ELECTRICAL ENGINEERING
ENGINEERING EXPERIMENT STATION
UNIVERSITY OF ILLINOIS
URBANA, ILLINOIS

ABSTRACT

Energy relations derived for a lossless closed uniform and periodic structure show that the total complex Poynting vector integrated over the cross section is identically zero for the case of an arbitrary complex wave. These results are also applicable to open structures provided certain conditions are satisfied. The application of these results in the field of leaky wave antennas is discussed. Two illustrative examples, those of the sinusoidally modulated reactance surface and the sheath helix, are worked out. It is shown that although the slope of the k-β curve can no longer be associated with the direction of net power flow, the knowledge of the slope may still be helpful in selecting certain modes for representing a given source.

Table of Contents

		Page
I.	Introduction	1
II.	Uniform Waveguide	1
III.	Periodic Structures	7
IV.	Open Waveguides	9
V.	Power Plots	10
VI.	Discussion of Power Plots	14
Acknowledgement		18
References		34

Illustrations

Figure 1	Waveguide Geometry.
Figure 2	k-β Diagram for SMRS.
Figure 3	Real and Imaginary Parts of $\mathcal{P}$ in SMRS for Real Γ.
Figure 4a	Real and Imaginary Parts of $\mathcal{P}$ in SMRS for Γ Complex.
Figure 4b	Real and Imaginary Parts of $\mathcal{P}$ in SMRS for real Γ Close to Turnover Point.
Figure 4c	Real and Imaginary Parts of $\mathcal{P}$ in SMRS for Γ Corresponding to Point C in Figure 2.
Figure 4d	Real and Imaginary Parts of $\mathcal{P}$ in SMRS for complex Γ Corresponding to ka=4.38.
Figure 5	k-β Diagram for Sheath Helix.
Figure 6	Real Parts of r. $\mathcal{P}$ in Sheath Helix for Real Γ.
Figure 7a	Real and Imaginary Parts of r. $\mathcal{P}$ in Sheath Helix for Γ Complex.
Figure 7b	Real Part of r. $\mathcal{P}$ in Sheath Helix for Real Γ in the Vicinity of Turnover Point.
Figure 7c	Real and Imaginary Part of r. $\mathcal{P}$ in Sheath Helix for Complex Γ in the Vicinity of Turnover Point.
Figure 7d	Real Part of r. $\mathcal{P}$ in Sheath Helix for (1) Real Γ in Mode 2 and (2) Real Γ in Mode 1 and Negative Slope.
Figure 7e	Real and Imaginary Parts of r. $\mathcal{P}$ in Sheath Helix for Complex Γ Close to Broadside Radiation Line in Mode 1.
Figure 7f	Real and Imaginary Parts of r. $\mathcal{P}$ in Sheath Helix for Complex Γ Close to Broadside Radiation Line in Mode 3.

I. Introduction

In this paper we derive the power and energy relations for uniform and periodic waveguides supporting a wave with a complex propagation constant in general. The study was prompted by the findings in an earlier investigation by the authors[1], in which it was shown that complex waves exist in a lossless isotropic waveguide possessing a glide reflection symmetry. Here the term complex wave implies a propagation constant $\Gamma = \alpha + j\beta$, with α the attenuation constant and β the phase constant, non-zero in general.

The relations appropriate to closed uniform waveguides have previously been derived by Chorney[2]. However, it is believed that the generalized formulation presented in this paper provides additional insight into the method of approach.

The authors have not come across the derivation of similar relations for periodic structures, or those applicable to open guides, uniform or periodic. These topics are discussed in sections 3 and 4 of this paper.

The paper also presents calculated power plots for two open guides, the sinusoidally modulated reactance surface and the sheath helix. These plots are discussed and some insight into the operation of the open guides as antennas is provided.

II. Uniform Waveguide

In this section we shall derive some energy relations in a uniform bidirectional waveguide. Chorney[2] was among the first to obtain the power and psuedo-energy theorems for such a structure. His formulation starts with the field distribution in the waveguide corresponding to a short circuit termination at a reference plane, say $z = 0$. These field expressions

are then substituted in a modified form of complex Poynting's theorem, which in turn leads to the desired relationships. Even though the artifice of a short circuit termination is used to derive the power and energy theorems, the end results obtained are for an infinite waveguide. Since the final result is independent of the termination, the motivation for using a short-circuit termination is not very clear. One of the purposes of this work is to investigate this question and to see if a satisfactory explanation for the method could be provided.

In the following, Chorney's power and pseudo-energy theorems are rederived using an arbitrary termination in the waveguide. This approach clearly explains the need for working with a general type of field expression in the formulation of the problem, one which is a superposition of the incident as well as the reflected field. The principal difference between the present formulation and that of Chorney lies in the generalization of the type of the termination in the waveguide.

Consider a uniform bidirectional waveguide filled with a lossless, homogeneous, nondispersive, and in general anisotropic medium, having permittivity and permeability tensors $\overline{\overline{\epsilon}}$ and $\overline{\overline{\mu}}$. Figure 1 shows such a waveguide geometry. The tensors $\overline{\overline{\epsilon}}$ and $\overline{\overline{\mu}}$ are hermitian and are shown in the following equation:

$$\overline{\overline{\epsilon}} = \begin{pmatrix} \epsilon_{11} & \epsilon_{12} & 0 \\ \epsilon_{21} & \epsilon_{22} & 0 \\ 0 & 0 & \epsilon_{33} \end{pmatrix}, \qquad \overline{\overline{\mu}} = \begin{pmatrix} \mu_{11} & \mu_{12} & 0 \\ \mu_{21} & \mu_{22} & 0 \\ 0 & 0 & \mu_{33} \end{pmatrix} \tag{2.1}$$

The modal electric and magnetic fields inside a uniform waveguide having an arbitrary termination, may be expressed as follows:

$$\bar{E}_t = \hat{E}_t\,(x,y) \left(e^{-\Gamma z} - R\, e^{\Gamma z}\right) \tag{2.2a}$$

$$\bar{E}_z = \hat{E}_z(x,y)\left(e^{-\Gamma z} + R\, e^{\Gamma z}\right) \qquad (2.2b)$$

$$\bar{H}_t = \hat{H}_t(x,y)\left(e^{-\Gamma z} + R\, e^{\Gamma z}\right) \qquad (2.2c)$$

$$\bar{H}_z = \hat{H}_z(x,y)\left(e^{-\Gamma z} - R\, e^{\Gamma z}\right) \qquad (2.2d)$$

A harmonic time variation $e^{j\omega t}$ is implicit in the above equations. Also, Γ is the propagation constant and is complex in general, i.e., $\Gamma = \alpha + j\beta$. The subscript "t" indicates a vector transverse to the z direction. Note that the field expressions contain both the incident and reflected terms. The reflection coefficient R is the description of the termination, referred to the plane at z = 0. It is assumed that the termination reflects a single mode only, the one under consideration here.

Apply the complex Poynting's theorem to a volume v enclosed by two cross-sectional surfaces S_1 and S_2 (see Figure 1) and the waveguide walls. Since the tangential electric field is zero on the waveguide walls, one obtains

$$\int_{S_1} (\bar{E}_t \times \bar{H}_t^*) \cdot \hat{z}\, da - \int_{S_2} (\bar{E}_t \times \bar{H}_t^*) \cdot \hat{z}\, da =$$

$$j\omega \left[\int_v \bar{H}^* \cdot \bar{\bar{\mu}} \cdot \bar{H}\, dV - \int_v \bar{E} \cdot \bar{\bar{\epsilon}}^* \cdot \bar{E}^*\, dV \right] \qquad (2.3)$$

Substitute (2.2) in (2.3) to obtain

$$P \left\{ (e^{-2\alpha z} - e^{-2\alpha(z+a)}) - |R|^2 (e^{2\alpha z} - e^{2\alpha(z+a)}) - \right.$$

$$\left. R(e^{j2\beta z} - e^{j2\beta(z+a)}) + R^* (e^{-j2\beta z} - e^{-j2\beta(z+a)}) \right\} =$$

$$j\omega \left[\frac{U_m^+ - U_e^+}{a} \left\{ (e^{-2\alpha z} - e^{-2\alpha(z+a)}) - \right. \right.$$

$$|R|^2 \left(e^{2\alpha z} - e^{2\alpha(z+a)}\right) \Big\} -$$

$$\frac{U_m^- - U_e^-}{j\beta} \left[\left\{ R\left(e^{j2\beta z} - e^{j2\beta(z+a)}\right) - R^* \left(e^{-j2\beta z} - e^{-j2\beta(z+a)}\right) \right\} \right] \qquad (2.4)$$

where we have used the following definitions:

$$P = P_1 + jQ_1 = \frac{1}{2} \int_{S_1} (\hat{E}_t \times \hat{H}_t^*) \cdot \hat{z}\, da \qquad (2.5a)$$

$$U_m^{\pm} = U_{ht} \pm U_{hz} \qquad (2.5b)$$

$$U_e^{\pm} = U_{ez} \pm U_{et} \qquad (2.5c)$$

$$U_{ht} = \frac{1}{4} \iint \hat{H}_t^* \cdot \bar{\bar{\mu}}_t \cdot \hat{H}_t \, da \qquad (2.5d)$$

$$U_{hz} = \frac{1}{4} \iint \mu_{33} \hat{H}_z^* \cdot \hat{H}_z \, da \qquad (2.5e)$$

$$U_{et} = \frac{1}{4} \iint \hat{E}_t \cdot \bar{\bar{\epsilon}}_t \cdot \hat{E}_t^* \, da \qquad (2.5f)$$

$$U_{ez} = \frac{1}{4} \iint \epsilon_{33} \hat{E}_z \cdot \hat{E}_z^* \, da \qquad (2.5g)$$

$$\bar{\bar{\mu}}_t = \begin{pmatrix} \mu_{11} & \mu_{12} \\ \mu_{21} & \mu_{22} \end{pmatrix} \quad ; \quad \bar{\bar{\epsilon}}_t = \begin{pmatrix} \epsilon_{11} & \epsilon_{12} \\ \epsilon_{21} & \epsilon_{22} \end{pmatrix} \qquad (2.5h)$$

Equation (2.4) is true for all values of R. Thus one may equate the coefficients of R on both sides to obtain

$$P\left(1 - e^{\pm 2\alpha a}\right) = j \frac{\omega}{\alpha} (U_m^+ - U_e^+) \left(1 - e^{\pm 2\alpha a}\right) \qquad (2.6a)$$

$$P\left(1 - e^{\pm j2\beta a}\right) = \frac{\omega}{\beta} (U_m^- - U_e^-) \left(1 - e^{\pm j2\beta a}\right) \qquad (2.6b)$$

Equating the real and imaginary parts of Equations (2.6) there follows:

$$P_1 \left(1 - e^{-2\alpha a}\right) = 0 \qquad (2.7a)$$

$$Q_1 (1 - e^{-2\alpha a}) = \frac{\omega}{\alpha} (U_m^+ - U_e^+) (1 - e^{-2\alpha a}) \tag{2.7b}$$

$$P_1 (1 - e^{-j2\beta a}) = \frac{\omega}{\beta} (U_m^- - U_e^-) (1 - e^{-j2\beta a}) \tag{2.7c}$$

$$Q_1 (1 - e^{-j2\beta a}) = 0 \tag{2.7d}$$

which are appropriate for the forward waves, i.e., those with the $e^{-\Gamma z}$ variation. Similar relations are readily obtained for the reflected waves.

It is interesting to note that the set of equations (2.7) are independent of the termination in the waveguide. One might therefore question the necessity of introducing the reflected wave in the formulation of the problem. The answer to this question is found by retracing the steps used to derive (2.6) from (2.4). If we let R equal to zero at the outset, the information contained in (2.6b) will be lost. As will be evident later, both (2.6a) and (2.6b) are necessary to derive the complete energy relations in the general case of a complex Γ. It should be noted that the set of equations (2.7) are valid for a general Γ. They are therefore applicable to all the three cases of propagating, evanescent, or complex waves.

The following explicit relations may be readily obtained from (2.7):

(a) Propagating Wave ($\alpha = 0$, $\beta \neq 0$):

$$P_1 = \frac{\omega}{\beta} (U_m^- - U_e^-) \tag{2.8a}$$

$$Q_1 = 0 \tag{2.8b}$$

$$U_m^+ = U_e^+ \tag{2.8c}$$

(b) Evanescent Wave ($\alpha \neq 0$, $\beta = 0$):

$$P_1 = 0 \tag{2.9a}$$

$$Q_1 = \frac{\omega}{\alpha} (U_m^+ - U_e^+) \tag{2.9b}$$

$$U_m^- = U_e^- \tag{2.9c}$$

(c) Complex Wave ($\alpha \neq 0$, $\beta \neq 0$):

$$P_1 = 0 \tag{2.10a}$$

$$Q_1 = 0 \tag{2.10b}$$

$$U_m^+ = U_e^+ \tag{2.10c}$$

$$U_m^- = U_e^- \tag{2.10d}$$

These results are the same as those derived by Chorney, who used a short circuit termination ($R = 1$) as a starting point of his formulation. However, they are included here for the sake of completeness and also because we shall have occasions to refer to them later when we discuss the periodic structures.

The physical interpretation of these energy relations appears in Chorney's work and we shall not discuss much of that aspect in this work. Only a few brief comments will be made here in connection with the most interesting case, that of the complex waves. Equation (2.10) shows that the complex Poynting vector for a complex wave is identically zero, hence the law of conservation of energy is not violated. Prior to the derivation of these relations, it was widely believed, that such waves do not exist in lossless uniform guides as they will violate the principle of conservation of energy. An interesting observation in connection with case (c) is that although it corresponds to the most general type of propagation constant, the energy relations are rather special, because P_1 and Q_1 are both identically zero in this case. Another remark concerning this case is that the presence of an anisotropic medium is not necessary for the existence of such waves, although one may get this impression from the generalized nature of the medium which is considered in the formulation.

III. Periodic Structures

We shall now consider the extension of the energy relationships derived above to the case of periodic structures.

Consider an infinitely long, lossless periodic structure with its axis along the z direction. Following Floquet's theorem, the fields in such a structure may be expressed as a sum of infinite number of space harmonics. Thus, one may write

$$\bar{F} = e^{-\Gamma_o z} \sum_{n=-\infty}^{\infty} \bar{F}_n(x,y)\, e^{-j\frac{2n\pi}{d} z} \tag{3.1}$$

where $\bar{F}$ represents either the electric or magnetic field vector, Γ_o is the complex propagation constant ($\Gamma_o = \alpha + j\beta_o$), and d is the period.

The transverse and longitudinal electric and magnetic field components in a periodic structure, with an arbitrary termination, may be expressed as follows:

$$\bar{E}_t = \sum_n \hat{E}_{tn}(x,y)\, (e^{-\Gamma_n z} - R_n\, e^{\Gamma_n z}) \tag{3.2a}$$

$$\bar{H}_t = \sum_n \hat{H}_{tn}(x,y)\, (e^{-\Gamma_n z} + R_n\, e^{\Gamma_n z}) \tag{3.2b}$$

$$\bar{E}_z = \sum_n \hat{E}_{zn}(x,y)\, (e^{-\Gamma_n z} + R_n\, e^{\Gamma_n z}) \tag{3.2c}$$

$$\bar{H}_z = \sum_n \hat{H}_{zn}(x,y)\, (e^{-\Gamma_n z} - R_n e^{\Gamma_n z}) \tag{3.2d}$$

where

$$\Gamma_n = \alpha + j\,(\beta_o + \frac{2n\pi}{d}) = \Gamma_o + j\,\frac{2n\pi}{d} \tag{3.2e}$$

The R_n are complex scalars and may be identified as the reflection coefficients of the nth harmonic referred to the plane at z = 0. Let the characteristics

of the lossless homogeneous medium filling the structure be described by the tensors $\bar{\bar{\epsilon}}$ and $\bar{\bar{\mu}}$. These tensors are assumed to be of the same form as in (2.1).

Now substitute the field expressions in (3.2) into the energy integral (2.3). Take the volume v as the region enclosed by the waveguide walls, and the two cross-sectional surfaces S_1 and S_2, which are located at integral number of periods apart. That is, if S_1 be located at z then S_2 is to be located at z + pd, p being an integer. This particular choice of the surfaces S_1 and S_2 is obvious from the periodic nature of the fields.

Let

$$P = P_1 + jQ_1 = \sum_{\substack{m=-\infty \\ m\neq n}}^{\infty} \sum_{n=-\infty}^{\infty} (P_{nm} + P_{nn}) \tag{3.3a}$$

$$P_{nm} = \frac{1}{2} \int_{S_1} (\hat{E}_{tn} \times \hat{H}^*_{tm}) \cdot \hat{z} \, da \tag{3.3b}$$

Notice that the above definitions are analogous to those in (2.5a) except now one has an infinite sum of integrals representing P_1 and Q_1 which include the self as well as mutual terms, P_{jj} and $P_{jk}(j\neq k)$. The pseudo-energy terms may also be defined in a manner similar to (2.5b) through (2.5g). Upon simplification it is possible to derive the energy relations exactly analogous to (2.6a) and (2.6b).

Without repeating the details of the derivations, which are quite similar to the uniform waveguide case, we shall simply state the important conclusions based on the above relations:

a) For a propagating wave ($\alpha = 0$, $\beta_o \neq 0, \pi/d$), the imaginary part of the complex Poynting vector integrated over the cross-section is identically zero, i.e., $Q_1 = 0$.

b) In the case of an arbitrary complex wave on the structure ($\alpha \neq 0$, $\beta_o \neq 0$, π/d), the integrated value of the complex Poynting vector is identically zero, i.e., $P_1 = 0$ and $Q_1 = 0$.

An important point in connection with the above results is that they hold true for the aggregate of the self and mutual terms, i.e., P_1 and Q_1, rather than for the individual terms P_{nm}. In fact, it has not been possible to derive explicit relations for the individual terms P_{nm}.

The special cases for the evanescent ($\alpha \neq 0$, $\beta_o = 0$), and the filter cutoff waves ($\alpha \neq 0$, $\beta_o = \pi/d$), occur in the region of transition on the k-β diagram where β_o goes from propagating to the complex wave region. However, P_1 and Q_1 still turn out to be zero at these points, as these may be considered as the limiting cases of the complex waves.

IV. Open Waveguides

So far we have restricted our discussion to closed waveguides - uniform or periodic. It is interesting to pose the question whether there exist energy relations similar to the ones derived above which are applicable to open waveguides. This topic will now be discussed briefly.

The principal difference between open and closed waveguides, is of course, the boundary condition at infinity. In deriving the energy relations for the closed waveguides, use was made of the fact that the tangential electric field was zero on the walls, and hence, there was no contribution of the Poynting vector on the wall surfaces. Clearly, the corresponding contribution from the surface at infinity will not be zero, in general, for a given open structure.

However, for a surface wave type of mode supported by an open structure, the fields have an exponential decay in the transverse direction, and the analysis presented above for the closed structures is equally well appli-

cable here. The surfaces S_1 and S_2, which are transverse cross-sections, are now necessarily of infinite extent. The main difference between the analysis of the uniform and periodic guides is the choice of the relative locations of S_2 with respect to S_1. In the uniform case the locations of S_1 and S_2 are arbitrary, whereas in the periodic case they must be separated by a distance which is an integral multiple of the period d.

An even more interesting frequency region in the open guide case is where the structure supports complex waves. Again, if in this region of frequency the transverse wave number is such that there is an exponential decay at infinity, the analysis given in the previous section continues to be valid. Complex waves that decay in the transverse direction are of backward type*. Open structures supporting such waves have been found useful in the design of log-periodic antennas, and the energy relations derived here provide considerable insight into the radiation mechanism of such antennas.

In order to discuss this matter further it will be useful to study the detailed behavior of the complex Poynting vector for some open waveguides. This task is undertaken in the following section.

V. Power Plots

In this section we present some graphs of the complex Poynting vector, $(\hat{E}_t \times \hat{H}_t^*) \cdot \hat{z}$, plotted as a function of the distance along the transverse direction. These calculations are for the sinusoidally modulated reactance surface (SMRS) studied by Oliner and Hessel[4], and for the sheath helix, the detailed analysis of which appears in Watkins[5]. The field expressions

*For a detailed discussion on backward and forward complex waves see Tamir and Oliner[3].

used in the calculation are reproduced here from the above two references and the interested reader is referred to them for further details.

(a) Sinusoidally Modulated Reactance Surface (SMRS).

The electric and magnetic fields on SMRS may be expressed as follows:

$$H_y = e^{-\Gamma_o z} \sum_{n=-\infty}^{\infty} \frac{I_n}{\sqrt{2\pi}} e^{-j\frac{2n\pi}{a} z} e^{-\tau_n x} \tag{5.1a}$$

$$E_x = e^{-\Gamma_o z} \sum_{n} j\beta_n \frac{I_n}{\sqrt{2\pi}} e^{-j\frac{2n\pi}{a} z} e^{-\tau_n x} \tag{5.1b}$$

where $\Gamma_o = \alpha + j\beta_o$, $\Gamma_n = \Gamma_o + \frac{j2n\pi}{a}$, $\tau_n = -j\sqrt{\Gamma_n^2 + k^2}$.

The surface reactance is of the form $X(z) = X_s [1 + M \cos (\frac{2\pi}{a} z)]$.

The difference equation satisfied by the coefficients I_n is:

$$I_{n+1} + D_n I_n + I_{n-1} = 0, \quad n = 0, \pm 1, \pm 2, \ldots \tag{5.2a}$$

where

$$D_n = \frac{2}{M} \left[1 - \frac{\tau_n}{X_s \omega \epsilon}\right] \tag{5.2b}$$

The characteristic equation for the propagation constant Γ_0 is obtained by setting the determinant of the infinite set of equations in (5.2a) equal to zero. This characteristic equation was solved for real and complex values of Γ_0, since complete information about Γ_0 required for the computation to be carried out, was not available from the reference cited above. Figure 2 shows two k-β diagrams, for $X_s' = 1$ and 5, and $M = 0.4$. $X_s' = X_s/\sqrt{\mu/\epsilon}$ is the normalized reactance of the surface. The values of Γ_0 were computed to the accuracy of three significant figures. The coefficients I_n corresponding to a given Γ_0 were next calculated from (5.2a), and I_0 was normalized to 1. With this data on hand, it is a straightforward procedure to compute the local Poynting vector, $\mathcal{P}$ ($= [\hat{E}_t \times \hat{H}_t^*] \cdot \hat{z}$), as a function

of the transverse dimension x. Using (5.1), $\mathcal{P}$ may be expressed as

$$\mathcal{P} = \sum_{m=-\infty}^{\infty} \sum_{n=-\infty}^{\infty} I_m I_n^* \Gamma_m e^{-(\tau_m + \tau_n^*) x} \qquad (5.3)$$

Figure 3 exhibits the real part of $\mathcal{P}$ as a function of the transverse dimension x, for the k-β combination determined by the point A marked on Figure 2. Since Γ_o here is purely imaginary the structure supports a propagating wave at this frequency. P, the total Poynting vector is represented by the area under the curve. This area turns out to be finite and positive as of course would be expected in this case.

Figure 4a shows the real and imaginary parts of $\mathcal{P}$ vs. the transverse dimension x. The propagation constant for this case is complex, as indicated by the point B in Figure 2. The integrated value of the complex Poynting vector is found to be zero, a result in agreement with the preceding theoretical derivations. It is interesting to note that the real part of the local Poynting vector is positive near the surface but rapidly becomes negative, and remains so, as one moves away from the structure.

Power computations have also been carried out for several values of the propagation constant in different regions of the k-β diagram for SMRS. These plots are presented in Figures 4b, 4c, and 4d. Some general comments based on these results will be advanced in the following section.

(b) Sheath Helix

Consider a sheath helix with a pitch angle Ψ, pitch p and radius a. The transverse electric and magnetic fields for the inside region of the helix ($0 \leq r \leq a$) are given by (for details see Watkins [op. cit.]):

$$E_r^i = \left[\frac{\Gamma}{\tau} C_n I_n'(\tau r) - \frac{n\omega\mu}{\tau^2 r} D_n I_n(\tau r)\right] e^{-\Gamma z} e^{jn\phi} \tag{5.4a}$$

$$E_\phi^i = \left[\frac{jn\Gamma}{\tau^2 r} C_n I_n(\tau r) - \frac{j\omega\mu}{\tau} D_n I_n'(\tau r)\right] e^{-\Gamma z} e^{jn\phi} \tag{5.4b}$$

$$H_r^i = \left[\frac{n\omega\epsilon}{\tau^2 r} C_n I_n(\tau r) + \frac{\Gamma}{\tau} D_n I_n'(\tau r)\right] e^{-\Gamma z} e^{jn\phi} \tag{5.4c}$$

$$H_\phi^i = \left[\frac{j\omega\epsilon}{\tau} C_n I_n'(\tau r) + \frac{jn\Gamma}{\tau^2 r} D_n I_n(\tau r)\right] e^{-\Gamma z} e^{jn\phi} \tag{5.4d}$$

$$\tau = -j \Gamma^2 + k^2$$

Similar expressions are obtained for the outside region $a \leq r < \infty$, when C_n, D_n, and I_n are replaced by A_n, B_n and K_n, respectively. Here I_n and K_n are modified Bessel functions, and the coefficients A_n, B_n, C_n and D_n are determinable from the solution of the characteristic matrix once the propagation constant Γ is known.

The determinantal equation for the sheath helix reads (see Watkins)

$$\frac{I_n'(\tau a)\, K_n'(\tau a)}{I_n(\tau a)\, K_n(\tau a)} = -\frac{(\tau^2 a^2 + jn\Gamma a \cot\psi)^2}{k^2 a^2 \tau^2 a^2 \cot^2\psi} \tag{5.5}$$

The real and complex solutions of this equation have recently been obtained by Klock.[8] A portion of the k-β diagram is reproduced here in Figure 5. The azimuthal variation was assumed to be of the form $e^{-j\phi}$ in his calculation.

The amplitude coefficients A_n, B_n, C_n and D_n may be calculated for given Γ by going back to the characteristic matrix. The complex Poynting vector in the z direction may then be obtained from the following:

$$\mathcal{P} = (E_t \times \hat{H}_t^*) \cdot \hat{z} = E_r H_\phi^*) - E_\phi H_r^* \tag{5.6}$$

Numerical computations have been carried out for the local Poynting vector $\mathcal{P}$ as a function of the radial dimension r. A few typical results

are presented in Figures 6, 7a through 7f where the product r.$\mathcal{P}$ rather than $\mathcal{P}$ itself is plotted. This is convenient because the integrated value of the Poynting vector over the cross section is directly obtainable from the area under the curve.

Figure 6 shows a plot of the real part of r.$\mathcal{P}$ vs. (r/a). This case corresponds to a value of Γ indicated by the point A in Figure 5, which is the case of a propagating wave. The real Poynting vector is found to be positive throughout.

Figure 7a shows the real and imaginary parts of r.$\mathcal{P}$ corresponding to the complex propagation constant Γ associated with the point B in Figure 5. It is again found, that the complex Poynting vector integrated over the cross-section is identically zero. It is interesting to note that the real part of the local Poynting vector is positive inside the helix while it becomes negative outside.

In the following section we shall present a brief discussion of the calculated power plots for the open waveguides.

VI. Discussion of Power Plots

We shall now present some observations based on the power plots of the two open waveguides discussed in the last section. Note first of all that in the pass-band region, where Γ is purely imaginary, the integrated Poynting vector is real and positive. However, locally the real part of $\mathcal{P}$ (= $\mathcal{P}_1$) may change from positive to negative as one moves along the transverse dimension. Although, this may not be obvious at first, a little thought will show that this is due to the fact that the power carried by various space harmonics, i.e., the P_{mm} terms, as well as the cross-flux terms P_{nm}, change considerably as one moves along the transverse direction.

This happens, for instance, at the frequency in the neighborhood of the point C in SMRS (see Figure 2), where the -1 space harmonic has the least decay in the transverse direction as compared to the others. By and large, the 0 and -1 harmonics are the two major contributors to the infinite sum representation for $\mathcal{P}_1$. The terms involving n = 0 are predominant near the reactance surface of SMRS making the net local power positive there. As one moves higher up in frequency and reaches a region corresponding to say, point B, (Figure 2), the integrated $\mathcal{P}_1$ is zero. The n = 0 terms are still predominant near the surface. However, the contributions of the terms involving the -1 space harmonic now become larger as well as more spread out in the transverse direction. This is because the amplitude of the -1 space harmonic has increased and its decay factor in the transverse direction has decreased in comparison to that at point C (Figure 2).

The power picture in the complex wave region leads to an interesting and useful interpretation of the radiation phenomenon in open waveguides. Suppose that an open waveguide is excited by a source located close to its surface. It is well known that the near fields due to such a source can often be described with good approximation by a complex wave supported by the structure. The corresponding field setup is such that the energy extracted from the source travels in the positive direction via fields closely attached to the surface, and is continually radiated into space by fields having a transverse distribution resembling the -1 space harmonic of the complex wave mode. The radiation is thus in the backward direction and the antenna is said to be backfire. The performance of such an antenna operating in this mode has a close resemblance to the two-line contradirectional coupler.

An interesting observation may be made for the stop-band region, say point D (Figure 2), where the propagation constant is also complex, but the power picture is radically different from that at point B.

Although the power plot for point D is not shown here, the real and imaginary parts of $\mathcal{P}$ are identically zero everywhere. Because of this, it is not possible to achieve efficient excitation or radiation from a waveguide operating in this frequency region.

The sheath helix, which is the other open waveguide structure for which the power calculations have been made, is slightly different from the SMRS. This is because its translation period is infinitesimally small, and hence, the field expressions appropriate to the sheath helix consist of a single traveling wave instead of an infinite number of space harmonics. In this respect it is similar to a uniform waveguide rather than a periodically loaded one.

One consequence of the above property of the sheath helix is that the stop-band ($\alpha \neq 0$, $\beta = \pi/d$) is absent in its k-β diagram. Except for this region, however, the power picture in the sheath helix is somewhat similar to that in SMRS when one considers the frequency regions which correspond to each other.

One important difference in the physical structure of the helix from the SMRS is, of course, that in the former there are two distinct regions separated by the helix surface. Thus, in the complex wave region of the helix, say at point B (see Figure 5), one notes from Figure 7 that $\mathcal{P}_1$ is positive inside and negative outside. However, it is not necessarily true for all complex wave regions that the power be negative in the entire outside region. For example, in the neighborhood of the point C (see Figure 5), the power is positive near the surface, but quickly changes to negative values as one moves out along the radial direction. Also, at point A (see Figure 5), the power is positive throughout; this behavior is similar to the SMRS.

The behavior of the tape helix, which is a more practical radiating structure, may be predicted quite well from the knowledge of the sheath helix power plots. The main difference between the two is, of course, the presence of the space harmonics in the tape version which are absent in the sheath. However, the power plots are expected to be quite similar.

The comments which were made earlier in connection with the open waveguides as radiators and the distribution of the power carried by the various space harmonics are generally valid in the case of the tape helix. It is well known that the bifilar tape helix in the push-pull mode is a good backfire antenna in the neighborhood of the onset of the complex wave region.

It has not been possible thus far to find a similar interpretation of the behavior of an open structure supporting a forward complex wave*. In the first place, these waves do not have a decay in the transverse direction, hence they do not satisfy the energy relations derived above. Some modifications in the approach are clearly necessary when dealing with such waves, but a satisfactory solution to this problem has yet to be found.

We shall close this section with one further comment. An interesting question which has frequently been posed is whether or not $dk/d\beta$ may be related to the direction of power flow in the complex wave region as it is possible to do when $\alpha = 0$. Since it has been shown that $P = 0$ for complex waves, the above question is not really very meaningful. However, a study of the power plots in various regions shows that the slope of the k-β plot may sometimes be related to the direction of power flow in certain local regions. This is particularly true for the region of transition from the

*For the properties of forward complex waves refer to Tamir and Oliner (loc. cit).

propagating to complex waves. At the onset of the complex wave region, and in its neighborhood, the power picture changes only slowly if the k-β diagram is also smooth there. Thus it is possible to predict the behavior of the local Poynting vector in the vicinity of the transition region from the knowledge of the nature of the plots just prior to entering the complex wave region. However, no general method of continuing the prediction has been found so far.

Acknowledgement

The authors are pleased to acknowledge the assistance of Mr. Glenn VanBlaricum in carrying out the numerical computations. The IBM 7094 computation facilities were provided by the Department of Computer Science through a grant from the National Science Foundation, NSFGP 700. The work carried out in this paper was supported in part by Wright Patterson Avionics Laboratory under contract AF33(657)-10474 and also in part by Cambridge Research Laboratories, Office of Aerospace Research, under contract AF19(628)-3819.

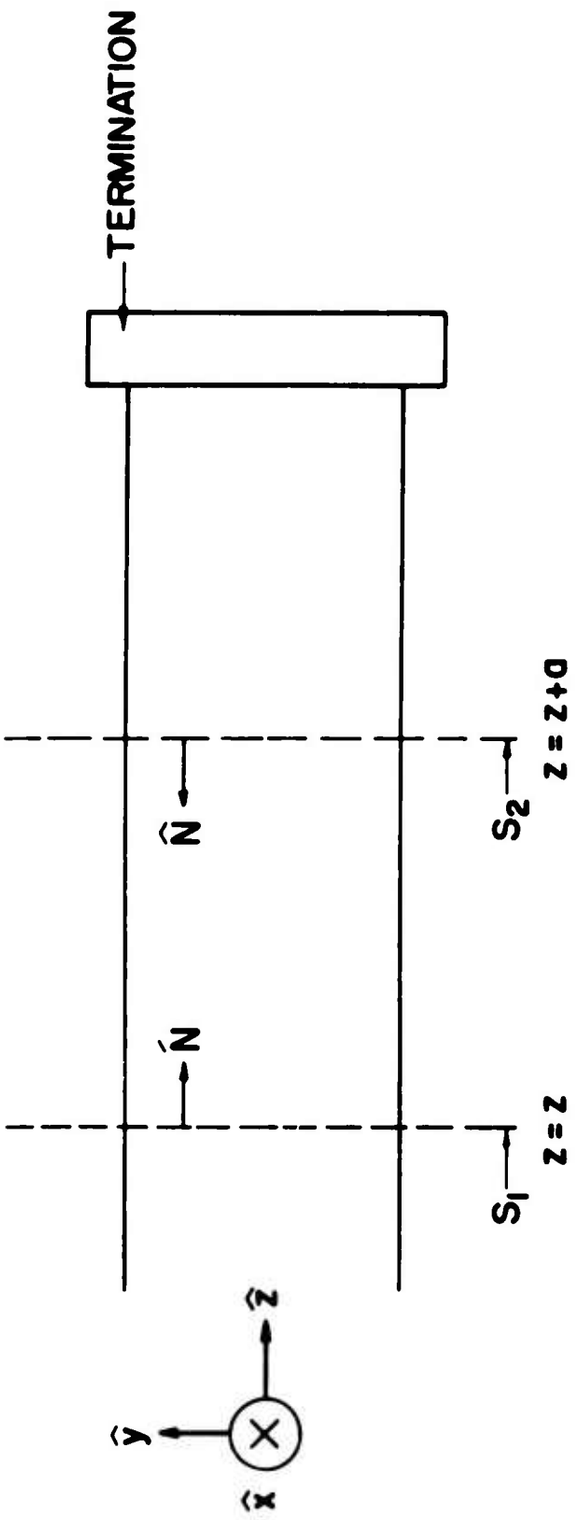

Figure 1. Waveguide Geometry.

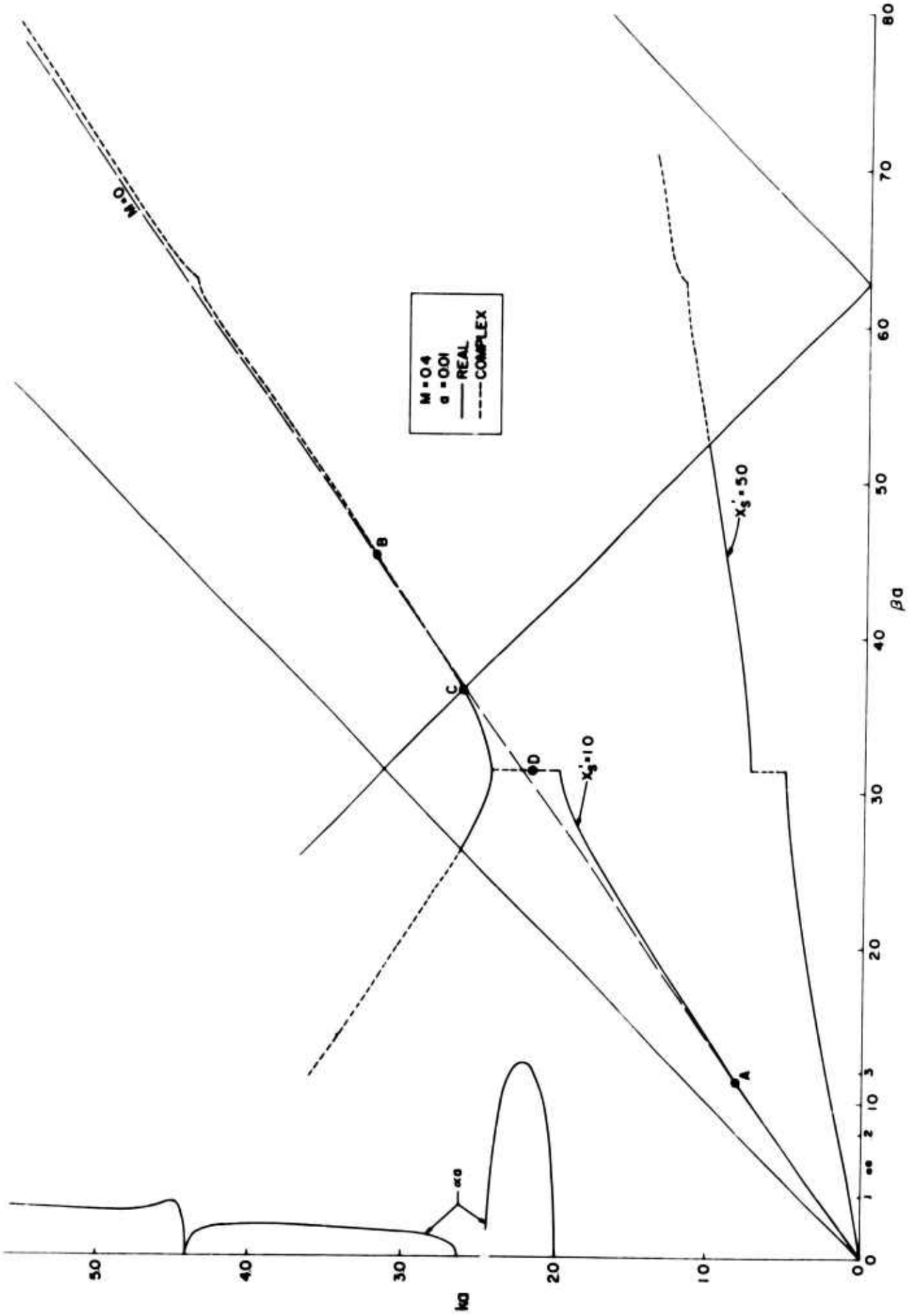

Figure 2. k-β Diagram for SMRS.

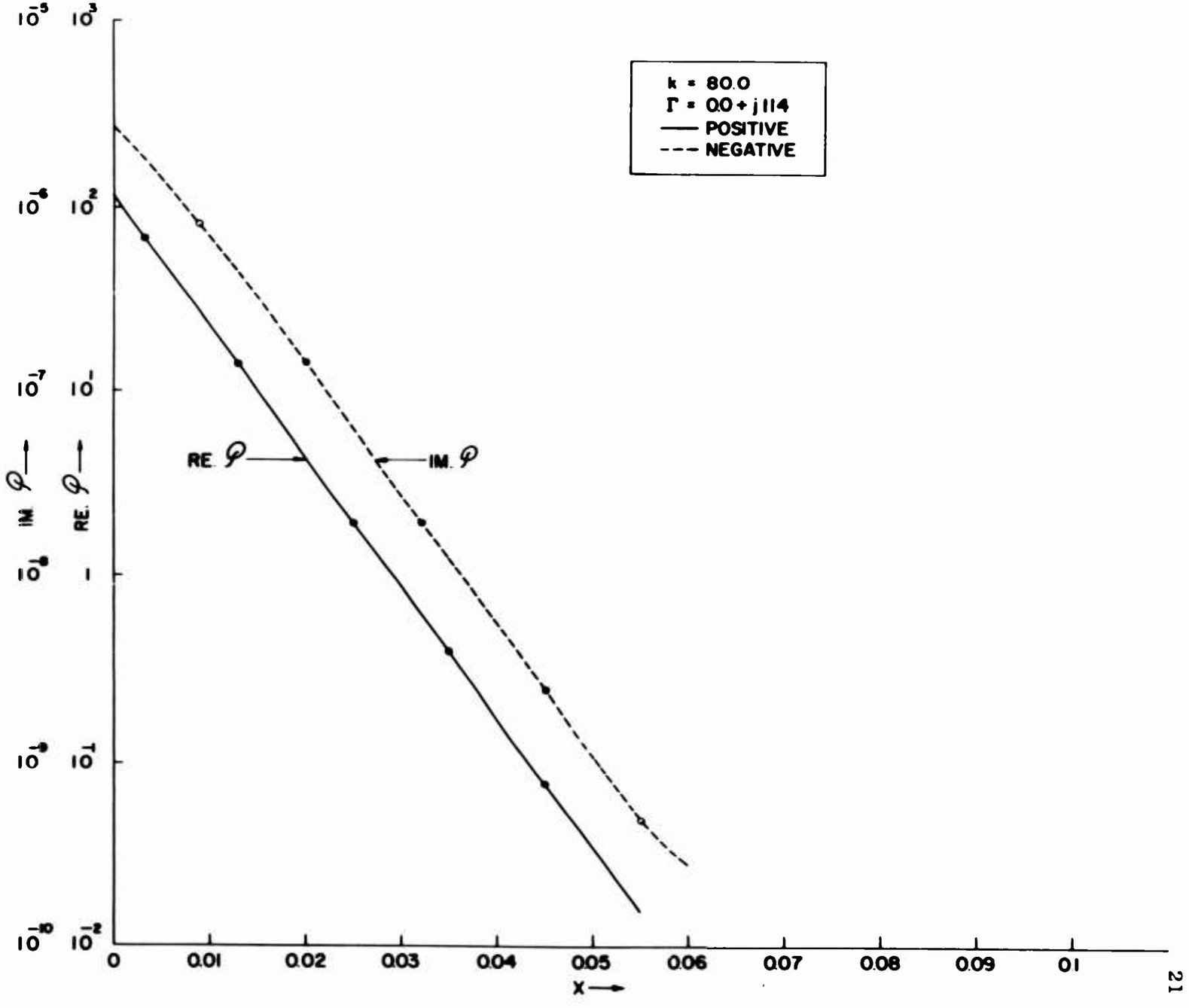

Figure 3. Real and Imaginary Parts of $\mathcal{P}$ in SMRS for Real Γ.

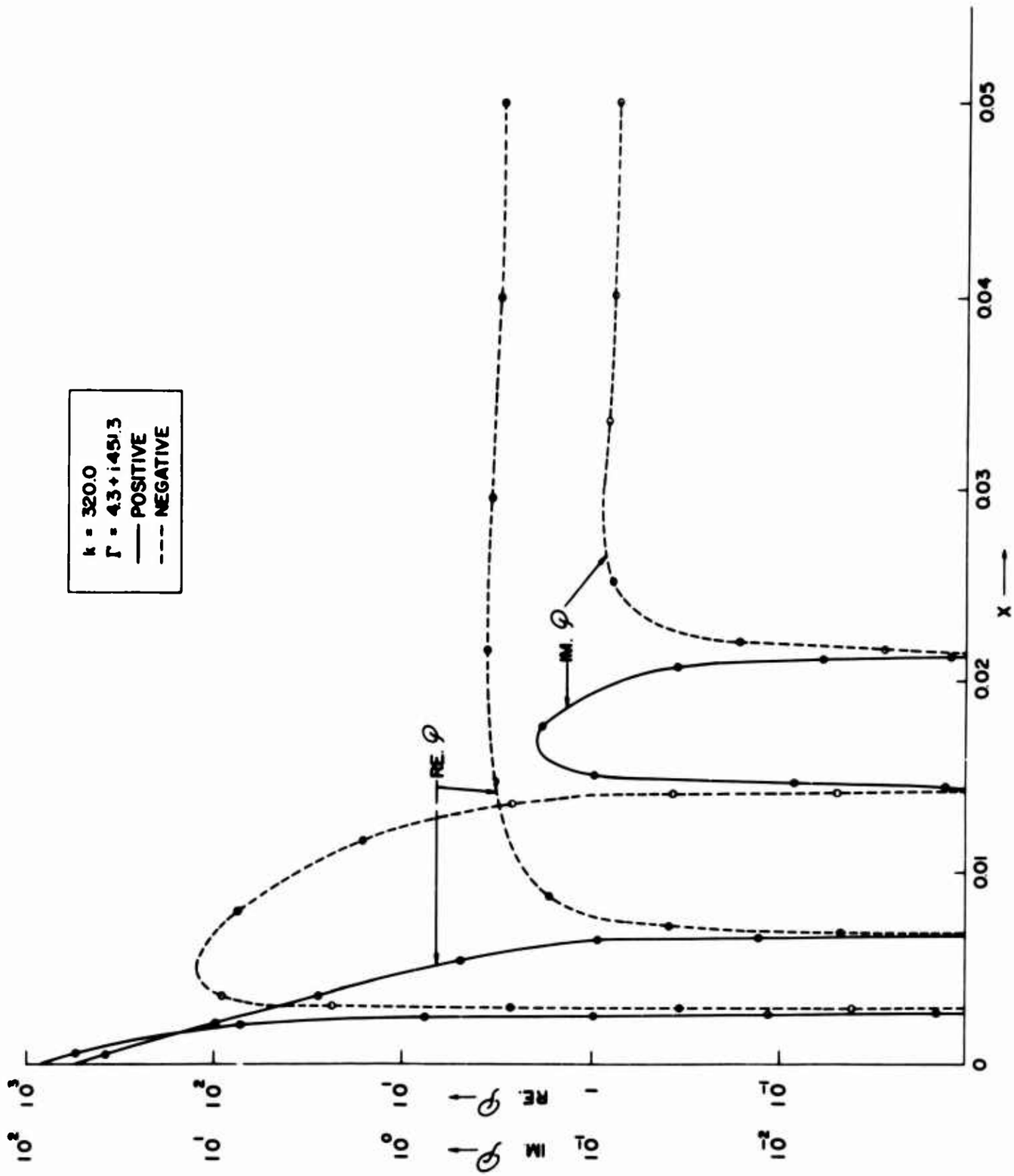

Figure 4a. Real and Imaginary Parts of φ in SMRS for Γ Complex.

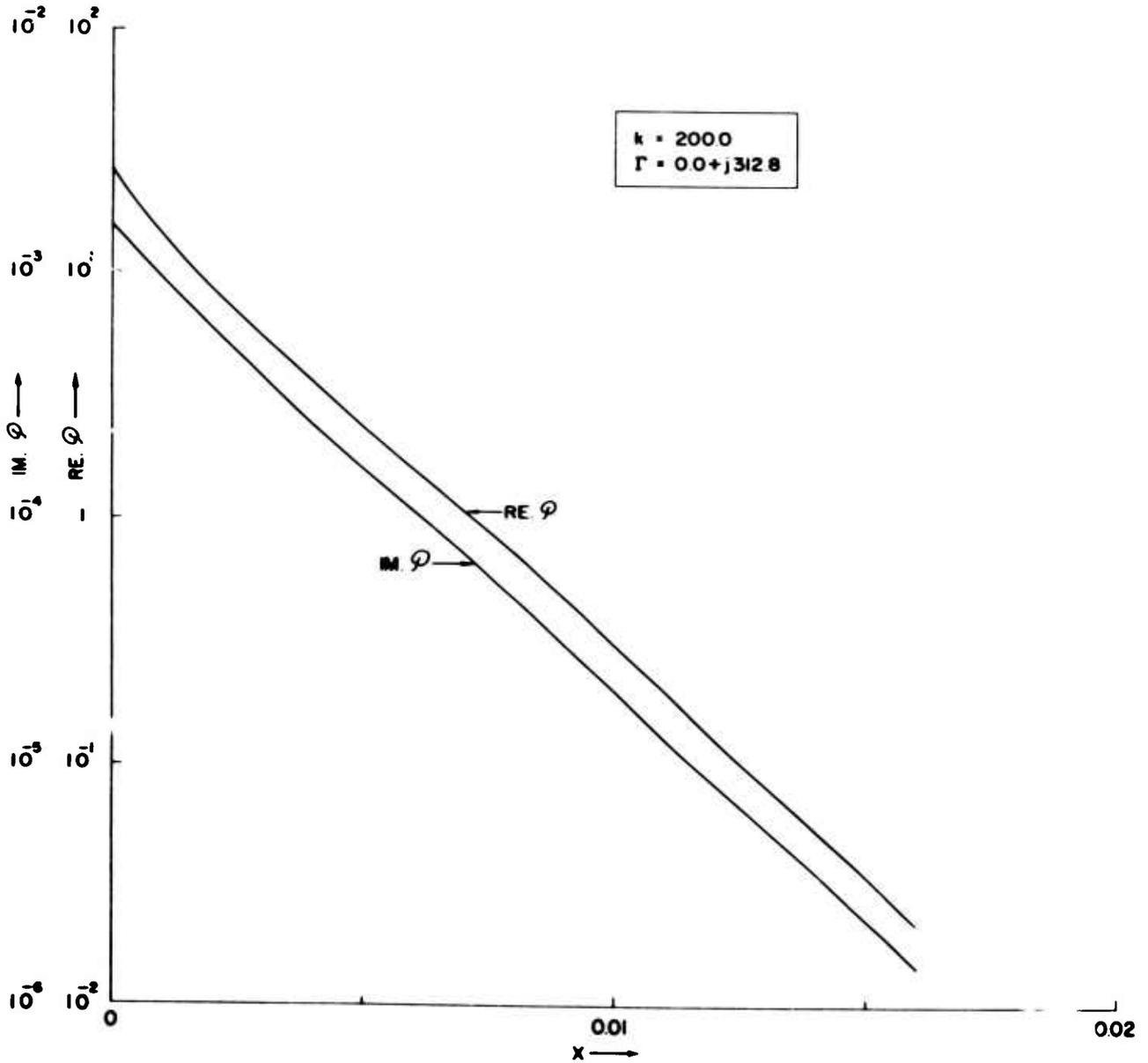

Figure 4b. Real and Imaginary Parts of $\wp$ in SMRS for Real Γ Close to Turnover Point.

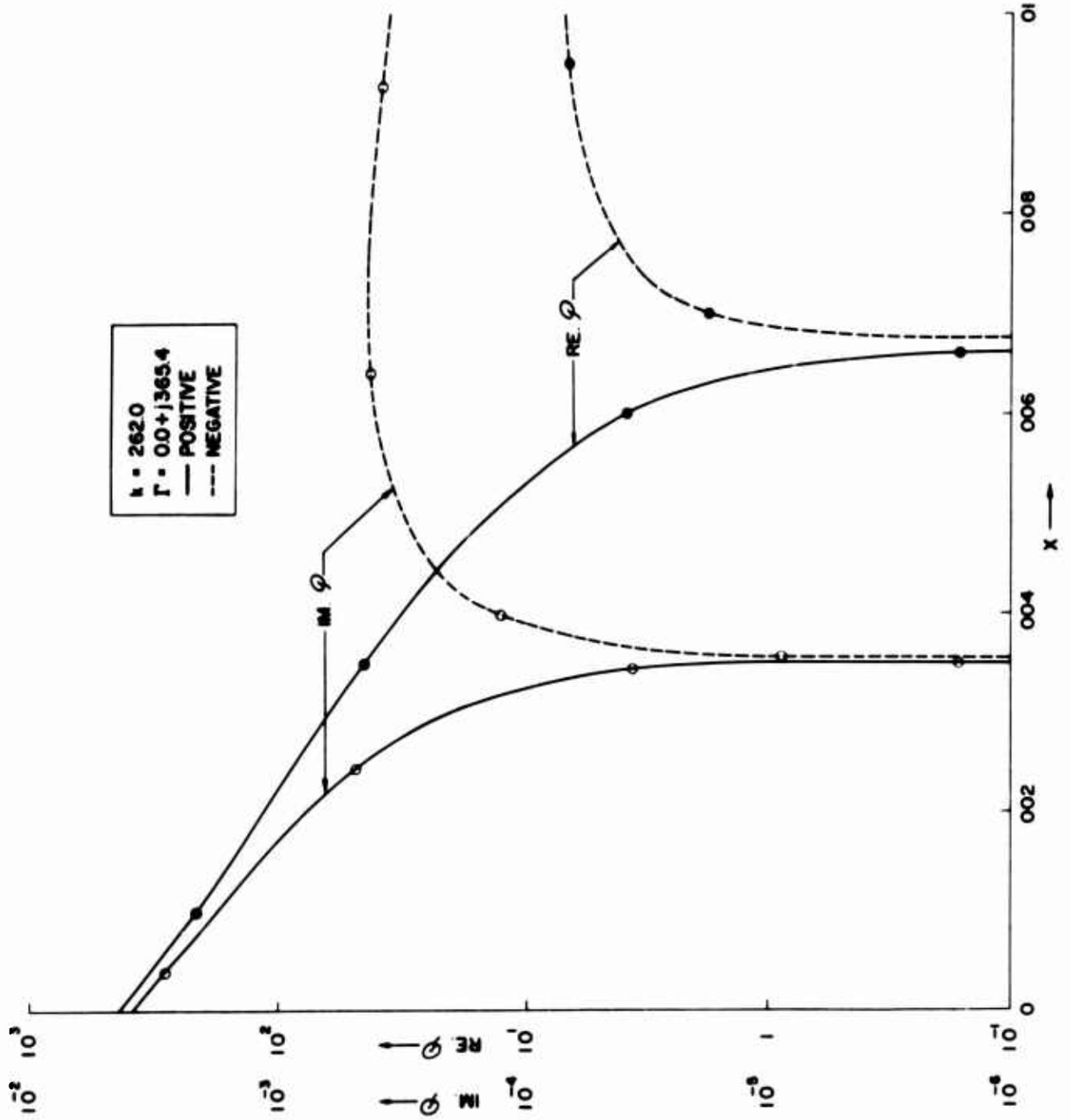

Figure 4c. Real and Imaginary Parts of ρ in SMRS for Γ Corresponding to Point C in Figure 2.

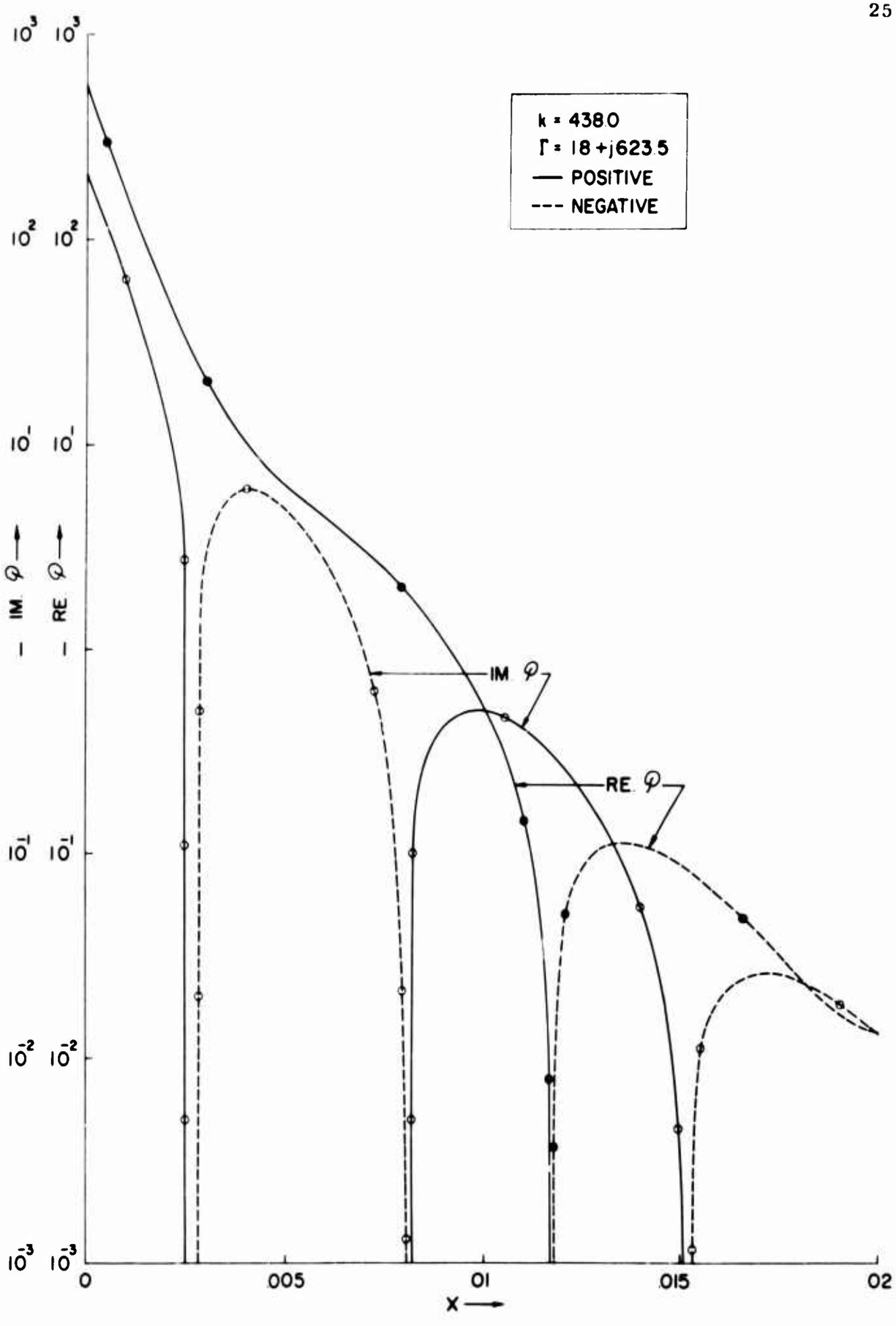

Figure 4d. Real and Imaginary Parts of $\mathcal{P}$ in SMRS for Complex Γ Corresponding to ka=4.38.

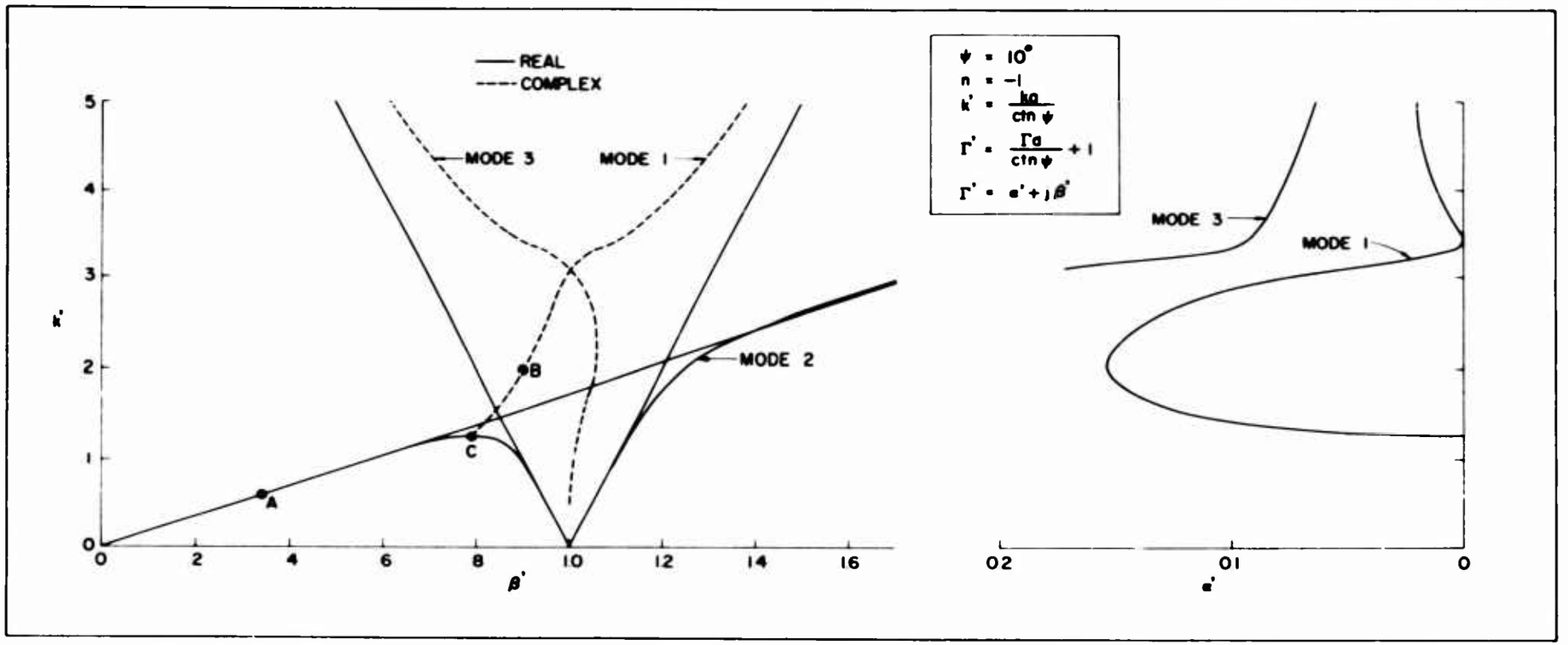

Figure 5. k-β Diagram for Sheath Helix.

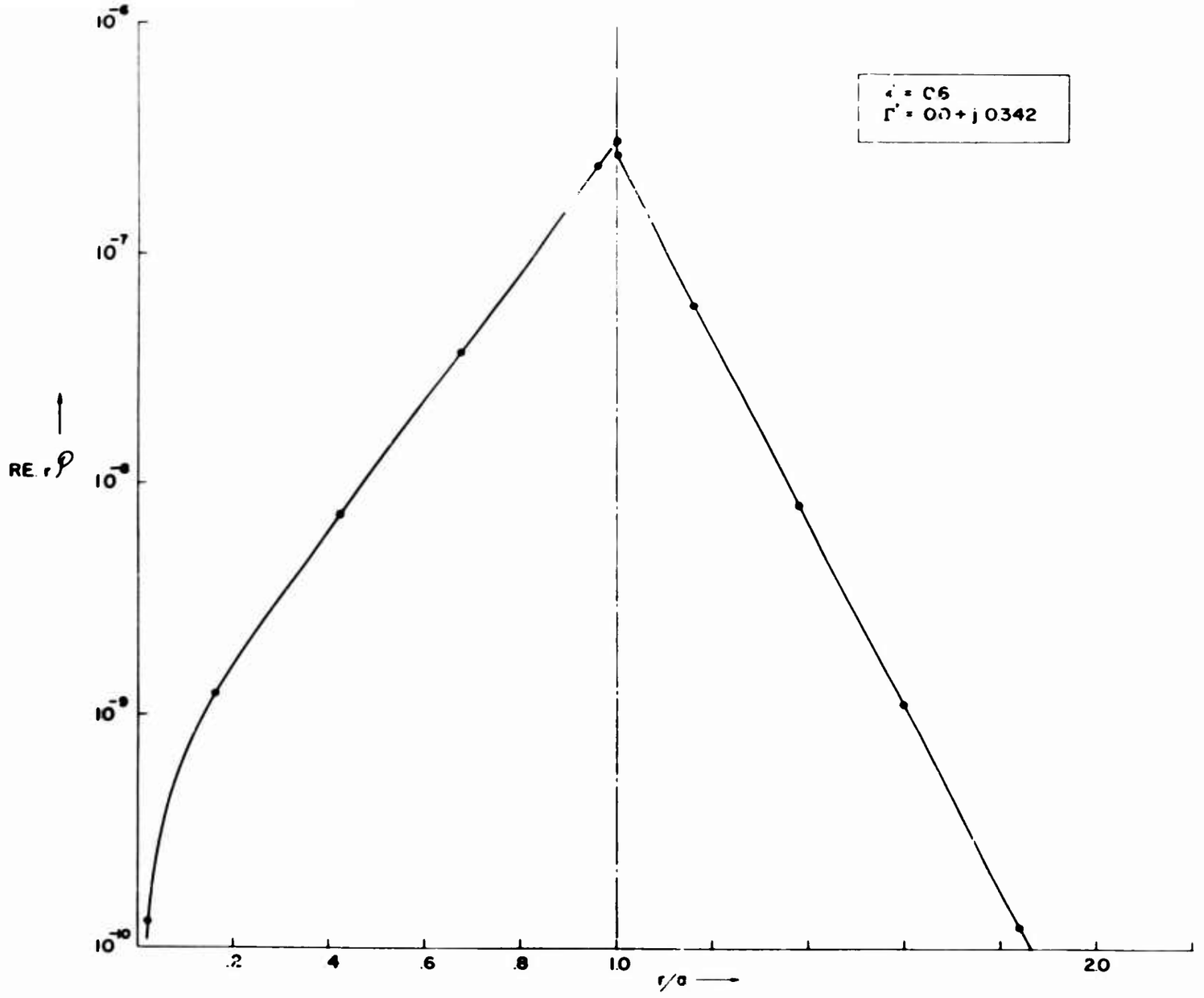

Figure 6. Real Parts of r. $\mathcal{P}$ in Sheath Helix for Real Γ.

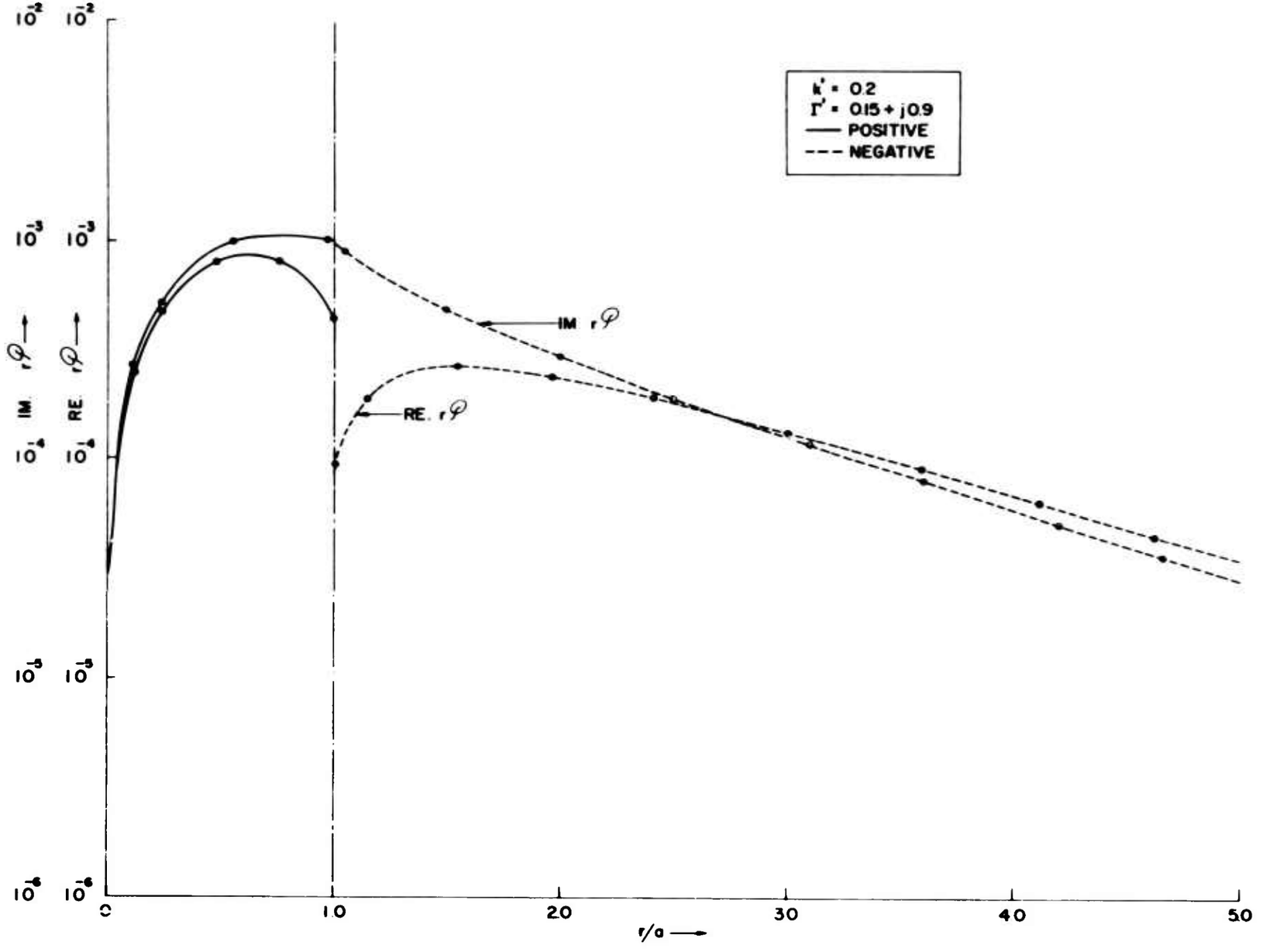

Figure 7a. Real and Imaginary Parts of r. $\mathbb{P}$ in Sheath Helix for Γ Complex.

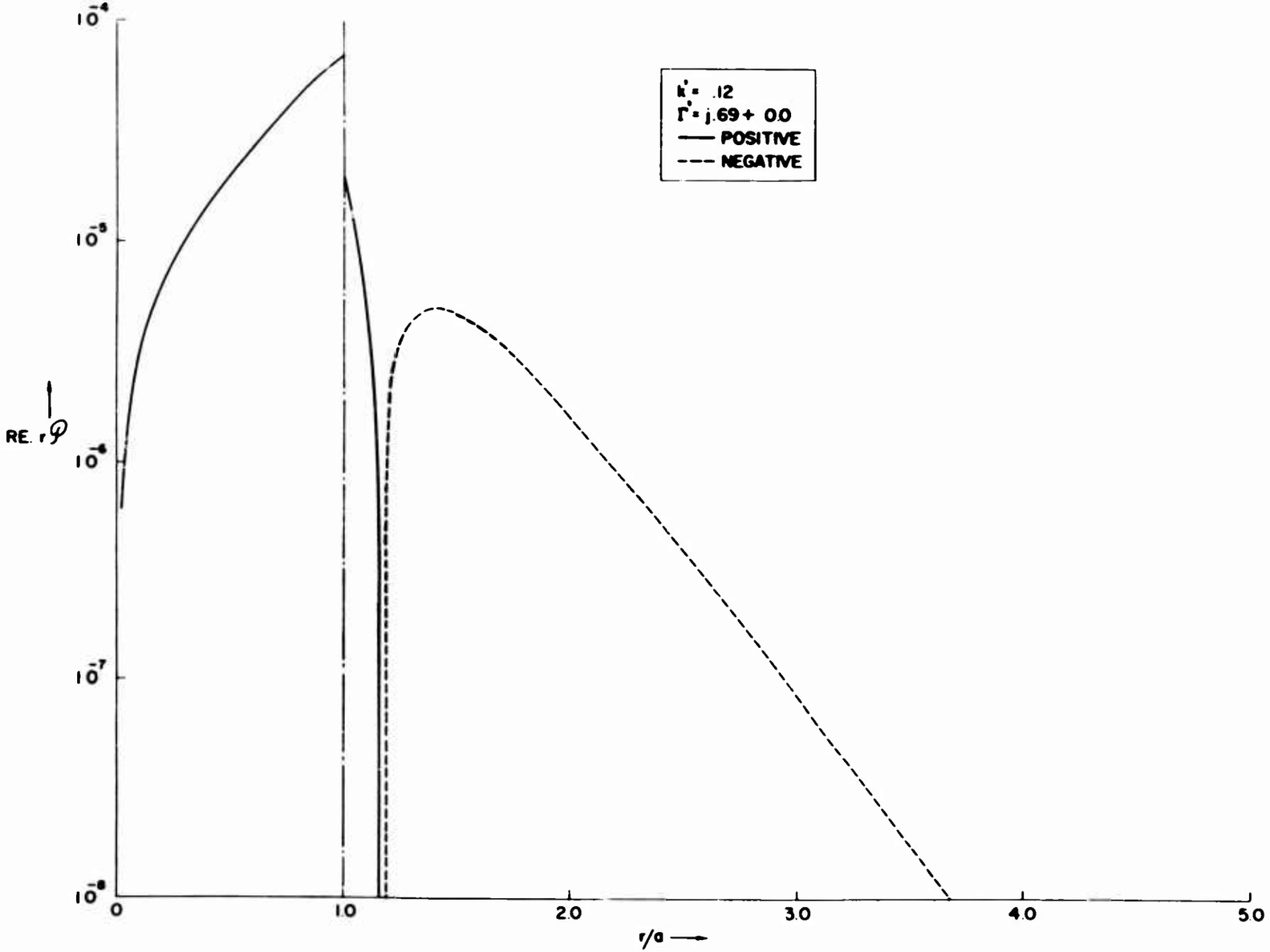

Figure 7b. Real Part of r. $\mathcal{P}$ in Sheath Helix for Real Γ in the Vicinity of Turnover Point.

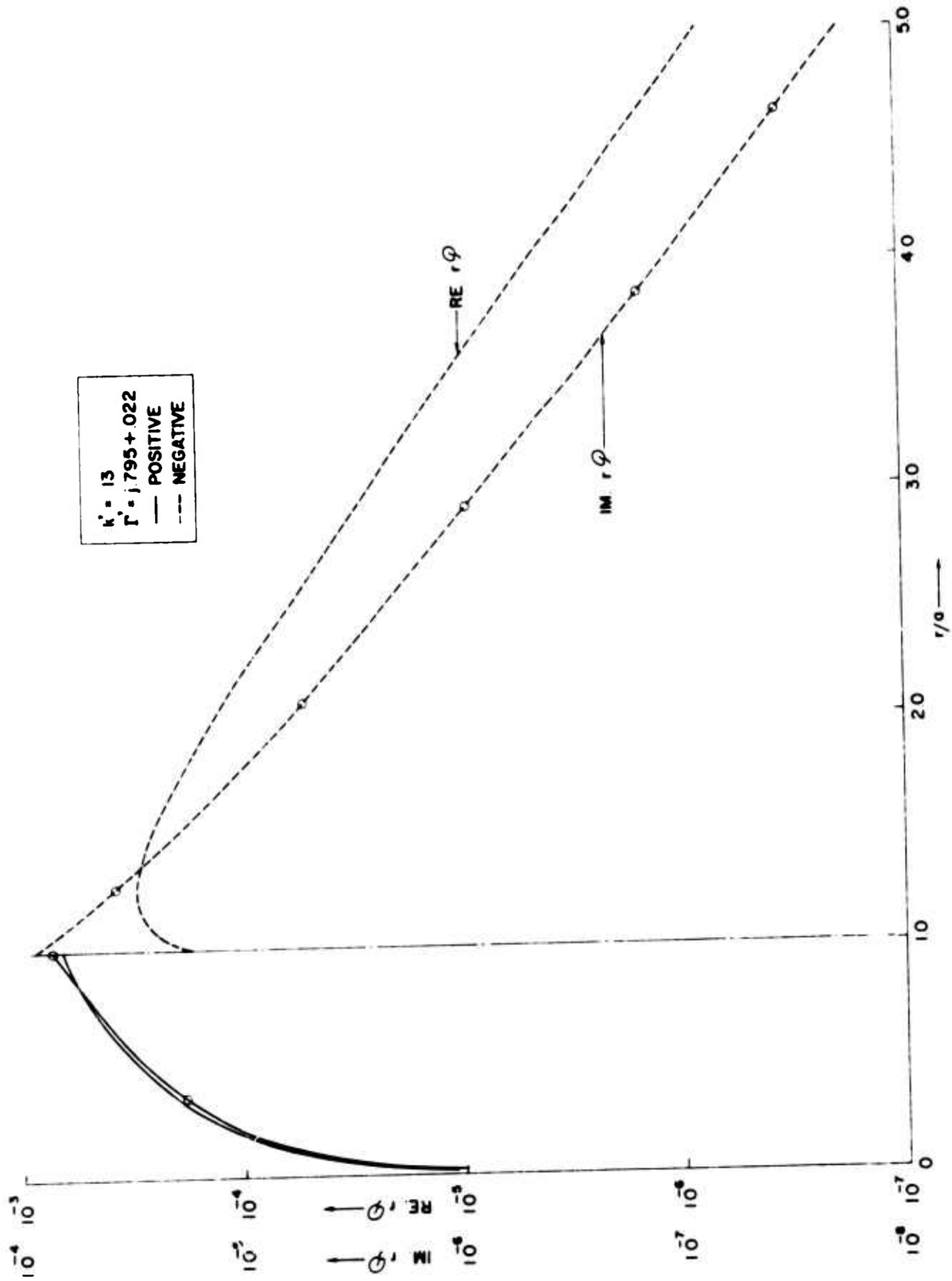

Figure 7c. Real and Imaginary Part of r. $\mathcal{P}$ in Sheath Helix for Complex Γ in the Vicinity of Turnover Point.

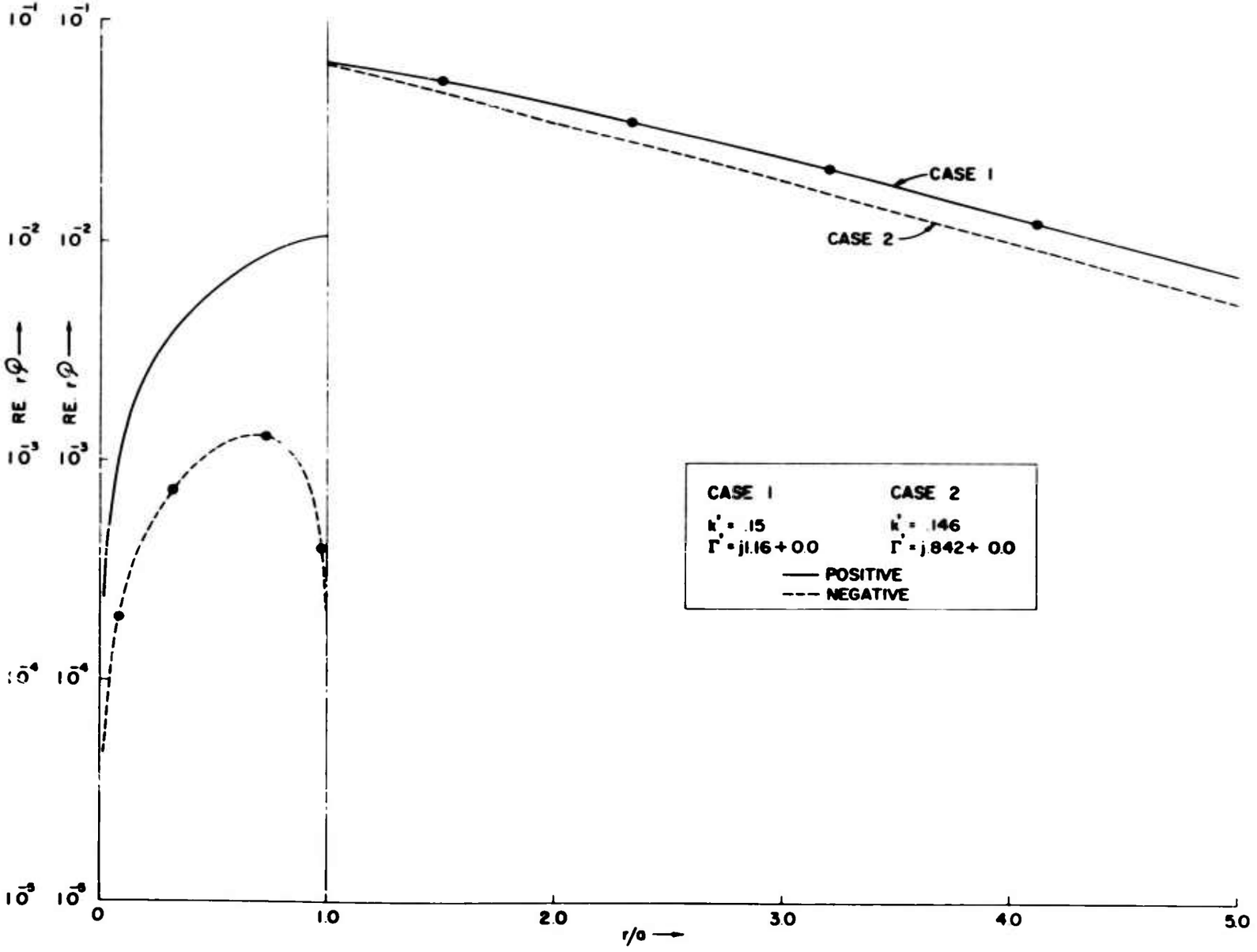

Figure 7d. Real Part of r. $\mathcal{P}$ in Sheath Helix for (1) Real Γ in Mode 2 and (2) Real Γ in Mode 1 and Negative Slope.

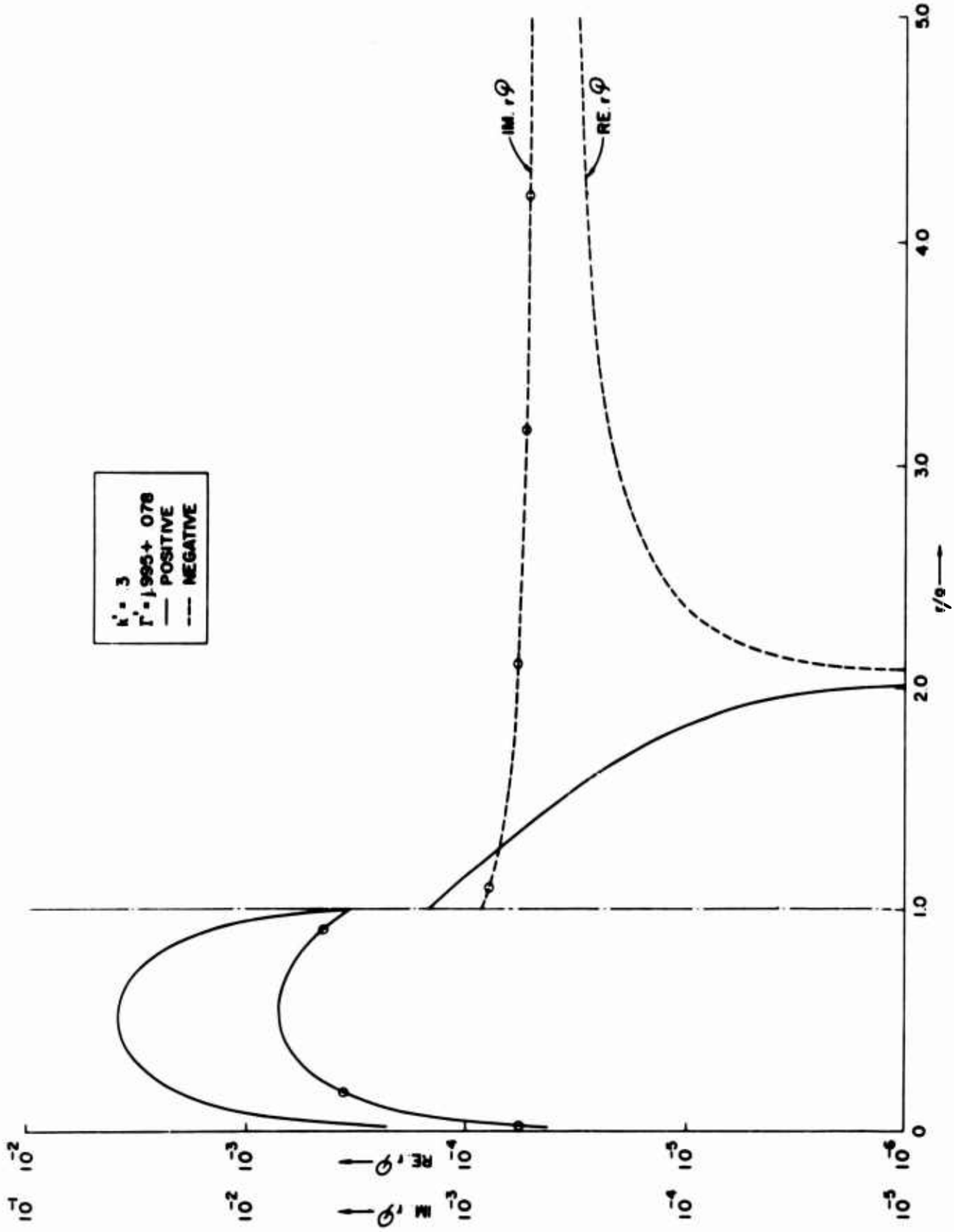

Figure 7e. Real and Imaginary Parts of r $\mathcal{P}$ in Sheath Helix for Complex Γ Close to Broadside Radiation Line in Mode 1.

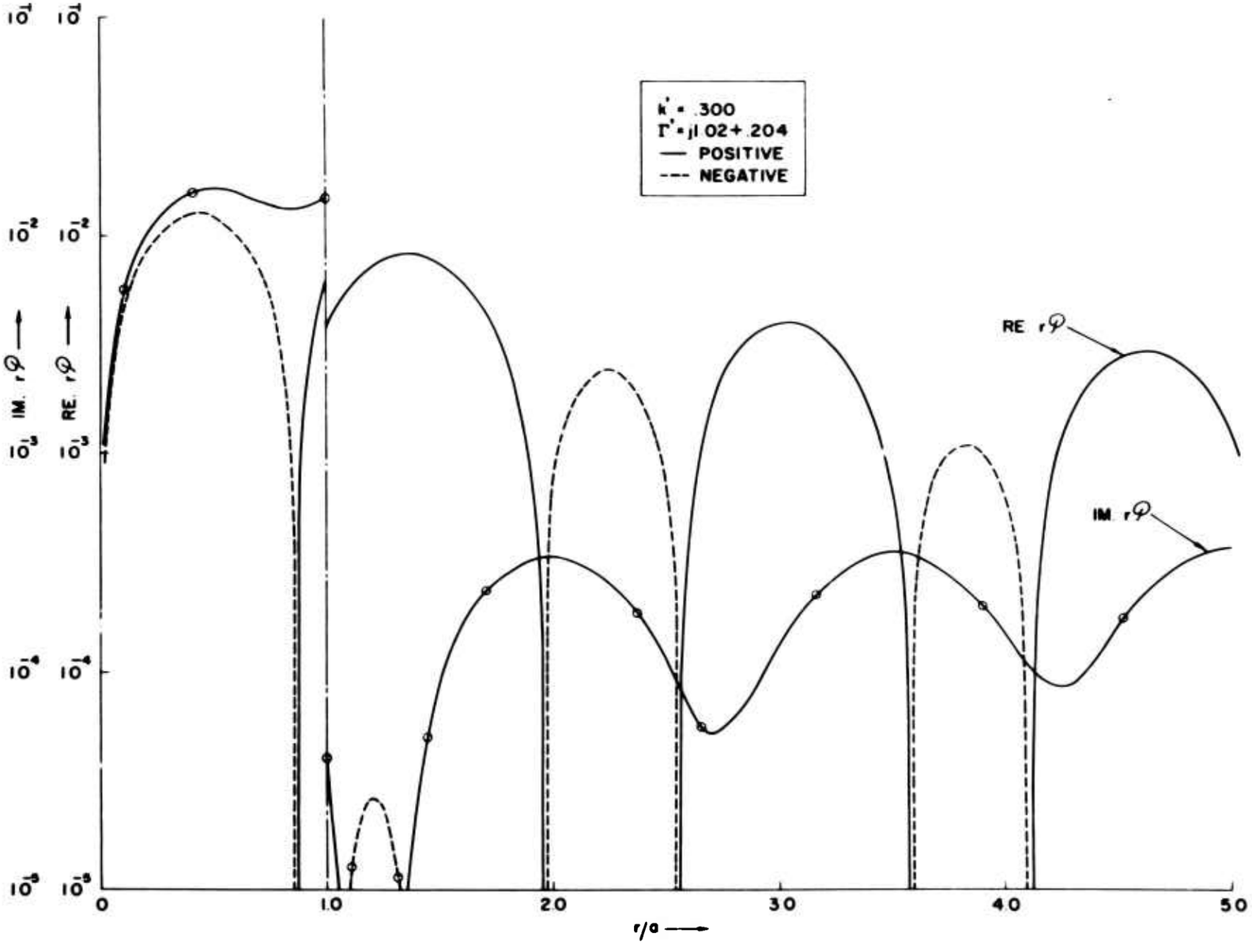

Figure 7f. Real and Imaginary Parts of r. $\mathcal{P}$ in Sheath Helix for Complex Γ Close to Broadside Radiation Line in Mode 3.

References

1. R. Mittra and S. R. Laxpati, "Propagation in a Waveguide with Glide Reflection Symmetry," Canadian Journal of Physics, Feb., 1965. Also see Tech. Report No. 75, Antenna Laboratory, Department of Electrical Engineering, University of Illinois, Urbana, Illinois, April, 1964.

2. P. Chorney, "Power and Energy Relations in a Bidirectional Waveguide," Symposium on Electromagnetics and Fluid Dynamics of Gaseous Plasma, Poly. Institute of Brooklyn, pp. 195-210, April 1961.

3. T. Tamir and A. A. Oliner, "Guided Complex Waves, Part I & II, "Proceedings IEE (London), Vol. 110, No. 2, February 1963, pp. 310-334.

4. A. A. Oliner and A. Hessel, "Guided Waves on Sinusoidally Modulated Reactance Surfaces," IRE Trans. PGAP-AP-7, Special Supplement, December 1959.

5. D. A. Watkins, "Topics in Electromagnetic Theory," John Wiley & Sons, Inc. 1958.

6. P. W. Klock, Private Communication.